Current injection phase thermography for low-velocity impact damage identification in composite laminates

S. A. Grammatikos[1], E. Z. Kordatos[1], T. E. Matikas[1], C. David[2], A. S. Paipetis[1]*

[1]Dept. of Materials Engineering, University of Ioannina, 45110 Ioannina, Greece

[2]TEI of Serres, Engineering Department, Serres, Greece

*e-mail: paipetis@cc.uoi.gr

Abstract

An innovative non-destructive evaluation (NDE) technique is presented based on current stimulated thermography. Modulated electric current is injected to Carbon Fibre Reinforced Plastics (CFRP) laminates as an external source of thermal excitation. Pulsed Phase Thermography (PPT) is concurrently employed to identify low velocity impact induced (LVI) damage. The efficiency of the proposed method is demonstrated for both plain and with Carbon Nanotubes (CNTs) modified laminates, which are subjected to low-velocity impact damaged composite laminates at different energy levels. The presence of the nano reinforcing phase is important in achieving a uniform current flow along the laminate, as it improves the through thickness conductivity. The acquired thermographs are compared with optical PPT, C-scan images and Computer Tomography (CT) representations. The typical energy input for successful damage identification with current injection is three to four orders of magnitude less compared to the energy required for optical PPT.

Keywords: Composites, Pulse Phase Thermography, Current injection, Low velocity impact damage

1. Introduction

Carbon /epoxy laminated composites are widely employed for structural elements in the aerospace industry due to their enhanced specific properties. Fibre reinforced laminates are suitable for complex geometrical applications, tailored mechanical behaviour and durability depending on the orientation of the layers of the laminate and the employed matrix. However, the anisotropy of advanced composite laminates leads to the initiation and propagation of different “damage entities”, often acting /interacting at distinct scales [1, 2]. The assessment of their structural integrity,

particularly in the presence of aggravating circumstances is of primary importance in order to secure airborne safety and cost efficiency.

The structural integrity of aircraft structures is primarily compromised by in-service fatigue [3]. Additional damage induced by incidental loads may become critical when interacting with cyclic loading. LVI is identified as an extremely hazardous cause of damage as it often induces damage invisible to the naked and may prove critical under certain circumstances [4]. LVI incidents may take place even during a scheduled maintenance service. When a LVI incident occurs, the induced damage tends to expand radially at the interlaminar faces, depending on the local strain energy release rate, which in its turn is governed by the relative change of the elastic properties as the laminae change orientation in the laminate [5].

LVI damage provides a challenging field for the application of a variety of non-destructive evaluation methods [5-8]. Of the many non-destructive techniques, Infrared Thermography (IrT) has proved its efficiency in defect identification and material characterization processes. IrT is a non-contact technique that provides full-field imaging which is fast and hence, cost effective [7]. With the appropriate stimulation energy, IrT provides thermal imprints of defects beneath the surface of materials giving a visual representation of the internal condition. A major technical difficulty for efficient damage identification with IrT is the uniform thermal excitation of the investigated structure in order to effectually pinpoint any present flaws [9-13].

Within the scope of this work, a novel thermal stimulation technique is developed. For this purpose, rectangular CFRP quasi isotropic plates were subjected to LVI. Two different energy levels were employed for LVI in order to assess the ability of the method to identify various defect sizes. Modulated electrical current was injected through the composite specimens in order to impose the necessary thermal gradient around the damaged area which was monitored using PPT. The anisotropic electrical conductivity and thermal diffusivity of the composite laminate makes the damage identification and quantification with PPT a challenging and demanding task. In this work, LVI induced damage was successfully identified for two impact energy levels and compared with typical optical IR stimulated PPT imaging ultrasonic imaging (C-scan), and CT representations of the cross sectional area of the impacted laminates.

2. Background

2.1 Infrared thermography

IrT is a thermal stimulation technique that identifies thermal variations on the surface of structures. Early research works [14, 15] identify the potential of these variations to reflect the structural state beneath the surface such as manufacturing flaws, delaminations, or cracks. IrT methods are

categorised in active and passive depending on the introduction of thermal stimulation. In the passive configuration, the structure is physically in higher temperature than the ambient and hence no external thermal excitation is needed. In the active approach, external thermal stimulation is employed to thermally excite the material surface, ideally in a uniform way. The presence of thermal gradients on the surface during (uniform) heating or cooling phase are potentially due to underlying damage or discontinuities and are manifested with local temperature extrema on a 2D representation, such as a thermal snapshot captured by the infrared camera [9]. Depending on the source and modulation of the thermal stimulation, a wide variety of different thermographic techniques may be employed. Step Heating Thermography (SHT), Vibration Thermography (VT), Pulsed Phase Thermography (PPT), Lock-in Thermography (LT) and Pulsed Thermography (PT) are typical examples of well-known thermographic techniques [9].

PPT is an active thermographic technique which offers phase and amplitude images of the inspected material. PPT is an inclusive combination of both Pulsed and Lock-in thermography [16]. It is a signal processing technique well developed by Maldague et al [17]. In this set-up, the structure is heated via a heat pulse. Thermal waves with various amplitude and frequency are generated in the near surface region (Fig.1) in the presence of flaws. The frequency content of these waves is subsequently analysed by the Fast Fourier Transformation (FFT) so as to acquire both phase and amplitude images [16, 18].

The attenuation of the thermal waves is highly sensitive to hidden defects and offers the possibility of quantitatively investigating various materials and structures. In Fig.1 the PPT concept is depicted. In this schematic representation, the stimulation source is performed optically using a flash lamp [9]. PPT exhibits characteristic advantages over other thermographic approaches, as it provides both amplitude and phase full field imaging. In this configuration, the amplitude images provide deeper probing whereas phase images are less dependent on surface features and non-uniform heating [17, 19]. Within the framework of the present study, heat excitation was provided by a square electric pulse injected in the bulk of the laminate with low frequency and thermal stimulation was achieved via the Joule effect.

2.2 Low-velocity impact damage in composite laminates

As aforementioned, LVI damage may cause the premature catastrophic failure of a structural element. This is mainly due to the reduction of the effective cross section of the laminate which makes it prone to buckling failure. LVI damage depends on many different variables. The “suspicious impactor” may come from a large number of adverse elements, vehicles, devices, tools

etc. The impacted area may be one of the many exposed regions to the many candidate impactors [5]. For most LVI incidents, the surface of the composite appears intact.

The laminated structure of an advanced composite is inherently responsible for LVI damage. Damage is usually manifested as blind interlaminar failure due to step changes in the elastic properties of the material in the through thickness direction [20]. In its turn, the matrix undertakes the role of sustaining interlaminar integrity or arresting further delamination [4]. Generally, there are two types of impact damage which are encountered in multi-layered laminates: the dynamic compression of the laminate cross section at the percussion front and the multiple delamination between the particular layers of the laminate. The type of the resultant damage is always a function of the fibre volume fraction, type of fabric and resin, fibre orientation of the particular layers as well as velocity, mass and geometrical characteristics of the impactor element [21, 22]. LVI initiates more pronounced delaminations at the interlaminar areas where there are major changes of the reinforcement direction [23]. In general, LVI induced composite damage is categorized into four main groups, matrix cracking, interlaminar failure (delamination), interfacial failure (fibre-matrix debonding) and fibre failure [5, 24]. Contrary to LVI, at high velocity impacts, fibre splitting and penetration are frequently encountered [24]. Fig.2 depicts intralaminar cracking and delaminations observed after a low velocity impact.

2.3 Current injection thermography

Many stimulation techniques have been developed in years with respect to active IrT. Ultrasound [25, 26], cyclic loading [10, 27], optical excitation (with incandescent or flash lamps) [25], or vibrations [9], are frequently employed as sources of thermal stimulation. Fundamental to a thermal stimulation protocol is the uniform excitation of the monitored surface for optimal detection of the emitted thermal waves with the simultaneous minimisation of the thermal energy input. Non-uniform thermal excitation impedes damage inspection. Large thermal energy input is energy consuming and overheating may degrade the primary structure (particularly in the case of CFRP, where the composite matrix temperature should be kept relatively low). In the case of periodic thermal loading, the energy input should allow for uniform heating of the monitored component. At the same time, a steady temperature state (compared to the excitation period) is not desirable, as the technique is based on the transient temperature profile monitoring.

An interesting approach to thermal stimulation is the exploitation of the conductive nature of CFRPs in order to use them as Joule heating elements. In general, the electrical properties of composite materials [28] and particularly of graphite /epoxy laminates have been widely studied for structural health monitoring or else real-time structural integrity assessment [29-32]. The Electrical Resistance

Change Method (ERCM) together with Electrical Potential Change Method (ERCM) is dealing with the electrical properties of the CFRPs in terms of damage monitoring [27, 28, 33]. It has been shown that reversible changes in the mechanical strain and irreversible service induced damage are reflected as changes in the electrical resistance or electrical potential, depending on the employed methodology [34-40]. Thus, the monitoring of the material electrical properties cumulatively provides a direct index of the intrinsic structural characteristics, the real time deformation state and the damage state. Apart from structural monitoring, the electrical properties of the carbon fibres have been exploited for curing carbon /epoxy materials [41], or even for tailoring the galvanic behavior at graphite/ aluminum interfaces in the case of composite aircraft repair [42, 43]. Joule heating has been employed for curing composite panels [44, 45] and for removing the ice from the skin of aircrafts [46]. Additionally to these studies, resistive heating of self-healing composites has been successfully applied in order to activate the "healing" process of the polymer matrix [47-50]. As stated by Fosbury et al [51], up to 100% energy conversion from electrical to thermal may be achieved.

It is now well established that the electrical properties may be improved through the incorporation of secondary conductive phases in the insulating matrix. One of the most widely employed methods is the dispersion of conductive Carbon Nanotubes (CNTs) in the epoxy matrix of the laminate [52-55]. It is reported that the inclusion of 0.5 % w/w CNTs in the matrix transforms it from an insulator into an electrically conductive or antistatic material [56]. More importantly, if the modified CNT epoxy is employed as the CFRP matrix, the laminate becomes conductive in directions other than those of the primary reinforcement, e.g. the through thickness direction [35].

When electrical current is injected through a bulk material it follows the lower electrical resistance path [35]. Current conduction is realized via (i) the primary reinforcement i.e. the carbon fibres (ii) via the secondary reinforcement i.e. the CNTs and (iii) via the random contacts of the reinforcing phases. These random contacts are loci of increased electrical resistance and therefore nuclei of heat generation. More random contacts result to a more uniform heat generation in the volume of the material [51]. As a result, the inclusion of CNTs results to a more uniform heating front on the laminate, as current traverses the laminate.

A carbon fabric layer may be represented as an array of electrical resistances (Figs.3a and b). The presence of any flaw, discontinuity or delamination reduces locally the electrical conductivity or even results to loss of electrical continuity. In this case, there is a preferential path of the electrical current via the route of maximum conductance. At the same time, as the electrical resistance at the damaged areas reaches high values, the joule effect should cause a temperature increase around the damaged region. This may be verified simply by assuming two cases of carbon fibre laminae: (i) a lamina with electrical resistance of $R_1 = R$ consisting of the resistances of the individual carbon

fibres laid in parallel and (ii) a second mechanically damaged layer with resistance (increased due to mechanical deformation or obstruction of the electrical path) R_2 = n*R (n>1). By employing the 1st law of thermodynamics, the Ohm's and Joule's law the following considerations are obtained:

$$P = \frac{Q+W}{t} \quad (1)$$

where P is the power (W), Q is the heat (J), t is the time (sec) and W (J) the work. In the case of electrical current injection through a material, the differentiation in the volume is negligible ($\Delta V=0$) and thus the work is zero. Hense, the power is:

$$P = \frac{Q}{t} \quad (2)$$

The Joule generated heat is given by:

$$Q = I^2 R t \quad (3)$$

where I is the electrical current (A), and R the electrical resistance (Ω).

From Eq.3 for the two particular cases:

$$P_1 = I^2 R_1 \quad (4)$$

$$P_2 = I^2 R_2 \quad (5)$$

By dividing Eqs.4 and 5 for given electrical current I and time t we obtain the following:

$$P_1 = \frac{1}{n} P_2 \text{ or } P_2 = nP_1, \text{ n>1} \quad (6)$$

From Eq.6 it is obvious that higher material electrical resistance results in higher power throughput and consecutively higher Joule heating. However, in the absence of electrical continuity there is no power throughput, In that case the "damaged" area is expected to remain cooler than the surrounding material. This temperature variation in the presence of a flaw is the "key point" of the proposed technique. The differentiation in temperature can be detected via the use of a thermal infrared camera. The novelty of the method lies on the fact that the local material properties will define the electrical current path and reveal the internal damage.

Considering electrical current injection, it is clear that appropriate electrical contacts are necessary in order to homogeneously distribute the current through the whole cross section of the bulk material. The minimization of contact resistance is indispensable in order to avoid Joule effects in the electrode/ material interface. These would inhibit the observation of damage induced temperature fluctuations. High contact electrical resistance results to a non-uniform thermal stimulation (hot edges - cooler central area) which may lead to unstable temperature gradients as well as catastrophic degradation of the epoxy matrix material due to overheating.

As should be added at this point, it is expected theoretically and shown experimentally [57] that for most materials including CFRPs, the temperature increase results to a proportional change of the

electrical resistance of the inspected material. However, carbon fibres possess a positive coefficient of thermal expansion (CTE) in the transverse axis and negative in the longitudinal, whereas typical epoxy matrices possess a positive CTE [58, 59]. This complicates the thermoelastic behavior of the composite. In general, temperature increase results to an electrical resistance increment (Eq.7):

$$R = R_0(1 + a(T - T_0)) \quad (7)$$

where R is the electrical resistance (Ω), R_0 the electrical resistance at room temperature conditions, (T_0 =20 ^{0}C), a the CTE (10^{-6} /^{0}C for carbon fibre) and T the temperature (^{0}C). Takahashi et al [60] examined the dependency of the electrical resistance of a graphite /epoxy polymer on temperature. They reported a 0.3% decrease in electrical resistance value in the reinforcement direction when the temperature increased from room conditions up to 60 ^{0}C. Concluding, typically the temperature increase is antagonistic to damage along the fibre direction. However, as was shown in previous studies, the resulting change in the electrical resistance is negligible compared to the local resistance change due to damage [32].

3. Experimental details

3.1 Materials

For the purposes of the study, $(0, 90)_{2s}$ six-layer cross-ply rectangular CFRP plates were fabricated using the hand lay-up method. Both plain and Carbon Nanotubes (CNTs) enhanced CFRPs were employed. The unidirectional carbon fabric 43280 (160 gr /m^2) by Hexcel (France) was employed as reinforcement and the Epocast 52 A/B epoxy system by Huntsman International LLC (Switzerland) as matrix. For the CNT enhanced laminates, 0.5% w/w CNTs were added in the epoxy matrix. Dispersion of the CNTs in the epoxy matrix was performed via sonication for 2 h using the ultrasonic processor UP400S (400 W, 24 kHz) by Hielscher at 50% amplitude. This dispersion protocol was found to yield optimal fracture toughness properties for 0.5% w/w CNT/matrix ratio [61]. Lamination was performed using wet hand lay-up. The curing cycle was 2 h in an oven under vacuum conditions (-700 mbar) at 95 ^{0}C. The final fibre volume fraction was approximately 50%, as measured by an optical microscope and image processing software for both laminates.

Square coupons of 60x60x1mm^3 dimensions were cut from the manufactured laminates (Fig.4a, 4b). Contact resistance was of prior importance [30], so special care was taken for the realisation of appropriate electrical contacts for the current injection. The edges where current would be injected were slightly ground with a 150 grit emery cloth in order to locally remove the epoxy matrix from the material surface. The material was thoroughly cleaned, first with deionised water and subsequently with acetone. The specimens were left to dry in an oven at 50 ^{0}C for 4 h in order to

remove any moisture. Silver paint (Fig.4c and 4d) was applied on the abraded cross sections in order to eliminate electrical contact resistance (Fig.4c-4f). The electrodes for the current injection were connected with the cross section of the coupons using silver loaded adhesive tape (Fig.4e and 4f). Further minimization of the contact resistances was achieved by applying 80 bar pressure on the specimen injection edges, a process that increased the contact area between the tape and the specimen and consequently decreased the contact resistance [62, 63]. For the employed geometry, a maximum value of 1 Ω resistance was chosen as a threshold for efficient current injection, in order to avoid overheating at the electrode contact area. The initial resistance measured at the edges of the coupon via the 2-probe method was approximately 2 Ω. After the pressure application, the resistance dropped to less than 1 Ω for both plain and CNT modified matrix specimens.

3.2 Impact damage

The LVI damage was induced using the CEAST 9340 drop-weight tower by Instron. A 1.5mm diameter semi-spherical impactor was employed. For impact testing, the specimens were appropriately clamped on the testing machine. The specimens were subjected to 3J and 4J impact energy. The employed impact energy levels were low enough in order to avoid penetration in all cases.

3.3 Non-destructive evaluation methodology

The Jade 510-CEDIP-MIR infrared camera was employed for the thermographic inspection. The IR camera employs a cooled indium antimonide (InSb) detector (3-5 μm), with a frame rate of 50-150 Hz and a focal plane array (FPA) pixel format of 320x240. A 50 Hz frame rate was selected for the present study. The thermal sensitivity of the camera is lower than 25mK at 25^0C and the resolution 0.001^0C. In order to render the emissivity (ε) of the specimen surface close to that of the black body (ε=1, for optimal recording of the thermographic signals), the monitored surface was painted with a black mat paint (ε=0.97).

The camera was employed in both live and pulsed phase mode. The experimental setup which was developed in order to perform the novel current injection thermographic technique is shown schematically in Figs.5 and 6. As current flows through the material, Joule heating induces a heat front which propagates from the edges (current injection locations) towards the centre (cooler locations).

For the live mode, 10A electrical current were injected to the specimens for 60 sec via the DC power supply and then the materials were left to cool down in air for another 150 sec. The current injection

was interrupted at approximately 60 ^{0}C maximum temperature. As was observed, after that temperature, the material reached steady temperature state throughout its surface and as a result, in the absence of temperature gradients, no internal features could be discerned. Under all circumstances, heating of the material to temperatures higher than 80 ^{0}C was avoided, as it could affect the properties of the epoxy matrix.

For the pulse phase mode, the camera was connected with a pulse generator through a lock-in amplifier. As can be seen in Fig. 6, the signal of the pulse generator was amplified through a DC amplifier. The infrared camera was positioned at appropriate distance from the coupon i.e. at approximately 30 cm. This distance corresponded to resolution of 0.180 mm /pixel. Amplitude and phase images were available during the thermal excitation of the CFRP materials. In this case, a square current pulse of fixed amplitude was injected for a fixed period of time in the specimens. In this case, various attempts were performed in order to assess the optimum electrical current input that would steadily heat the materials with simultaneous minimisation of the required energy input. Finally, an amplitude of 200mA (0.5 V electrical voltage) for 50 seconds was chosen as excitation so as to uniformly induce thermal waves upon the specimens. As should be noted, the PPT current injection configuration was successful in identifying LVI damage with considerably less current amplitude.

Both ultrasonic C-scan and Computer tomography were employed in order to evaluate the impact induced damage on the composite laminates. The employed C Scan setup was a Single bridge ultrasonic immersion system (Physical Acoustics) with 3 computer controlled axes (x, y, z) and manual gimbal and swivel, 1μm step size, computer controlled P/R, high-speed A/D converter with 100Msps digitizing rate. For the Computer Tomographic Imaging, the Werth TomoScope® HV Compact Multi-Sensor Coordinate Measuring Machine with X-ray Computed Tomography for measurement of large parts and components with high density (Max. part dimensions Ømax.= approx. 327 mm; L= approx. 517 mm (depending on the aspect ratio of the components)

5. Results and discussion

As aforementioned, both plain and CNT modified materials were subjected to 3J and 4J impact damage. The recorded force vs. time curves are depicted in Figs.7a, 7b, 7c and 7d. The evaluation of the impact performance of the laminates is not within the scope of this study, although the presence of the CNTs is expected to enhance the interlaminar, fatigue and impact properties of the composite [57, 64-66]

Initially, the thermographic inspection was performed in “live” mode [18]. The 2D temperature distribution on the plate surface was simply recorded as a function of time. The material thermal response was recorded with the thermal camera, as both plain and CNT enhanced specimens were heated with resistance heating. In Fig.8 the employed thermal stimulation protocol is shown.

Fig.8 depicts the temperature profiles (normalized to the initial mean value) of both CNT enhanced and plain matrix CFRPs. The series of thermographs shown were recorded during the heating (top series) and cooling (down series) phase. As was observed, delamination damage was more easily identified during the current injection i.e. the heating process, as around the damaged area, a temperature gradient on the specimen surface was observed; after the interruption of current injection, i.e. during the cooling process, impact induced discontinuities on the specimen were less discernible. This effect was attributed to the fact that, during the current injection, heat was preferentially generated along the injection path, whereas during the cooling down process, heat was dissipated along all edges of the monitored surface. As the specimen was a typical symmetric cross ply laminate, the aforementioned effect could not be attributed to the symmetry of the lamination, i.e. the thermal anisotropy of the material along its surface [58, 59].

It is worth mentioning at this point, that conventional IR active thermography is more efficient in identifying discontinuities during the cooling phase [67]. In contrast, current injection thermography is more efficient during the thermal simulation, a fact that is attributed to the preferential introduction of the thermal energy in the material. The above thermographs show that (i) the temperature distribution was practically symmetrical to both the mid width horizontal and vertical axes of symmetry of the plate and (ii) the delaminated area is optically enhanced by elliptical cold areas which lie on the same vertical axis as the delamination itself which coincides with the current injection axis.

More importantly, the addition of the CNTs is considerably enhancing the aforementioned effect. As is reported from previous studies, although the electrical conductivity remains practically the same along the conductive carbon fibres, it is at least an order of magnitude higher in the through thickness direction [29]. It can be postulated that, as the addition of the CNTs is globally enhancing the electrical conductivity in the through thickness direction, it is also facilitating the homogeneous heat transfer induced via the Joule generated heat between the individual laminae. In the absence of the conductive nanophase, through thickness conductivity is solely dependent on the carbon fibre random contacts[30]. These contacts introduce random heat sources in the laminate which are independent of the current injection direction and mask the characteristic “butterfly pattern” observed in Fig.8 (heating phase).

Subsequently, PPT was employed with the purpose of defining the liming resolving ability of the proposed methodology while keeping the injected current at a minimum value, so as to minimize the effects of the joule heating on the impacted laminates. Figs.9 to 12 show in sequence (a) the top (impacted) side, (b) the bottom side, (c) the C-scan image (d) the thermal IrT phase image (e) the thermal IrT phase image with optical excitation and (f) the CT representation of the impacted cross section for both the 3J and 4J impact damaged plain and CNT modified CFRP coupons. Figs. 9-12c show the typical c-scan representation which as expected identifies the impacted region in all cases. The CT representations of the impacted cross section (Figs 9-12f) indicate the characteristic type of impact induced damage with a barely visible damage on the impacted side and much more prominent on the opposite side of the laminate. As Figs.9d, 10d, 11d and 12d illustrate, the induced damage is identified with the proposed method even with the minimum current excitation (200 mA). With the employed current injection protocol, the signal to noise ratio as indicated by the step intensity change in the perturbation area is more than 3, even in the case of 3J impact damage. As is obvious, better resolving ability may be achieved with higher current injection protocols, as was performed in the case of "live" thermographic monitoring (Figs 7 & 8).

It is evident that higher impact energy results in wider damaged area. Delaminated regions are almost visible in the cases of 3J impact energy (Figs.9, 11 (a, b, and e)). However, significantly severe damage was induced by the 4J impact enforcement (Figs.10, 12 (a, b, c and e)). For reference purposes, IR excited optical PPT was performed using 2 optical lamps of 1 kW each (Fig.9e, 10e, 11e and 12e). In that case, the materials were heated for 10 sec (square pulse) with 5V energy. As is obvious, phase images observed by resistive heating (Figs.9d-12d) are similar to the phase images when stimulating with the optical lamps (Figs.9e-12e). The inspection of the IR optical PPT phase images reveal clearly the locus of the LVI damaged area. The current injection thermographic system for the inspection of LVI damage is providing considerable potential as (i) it does not require an external heat source as the material is directly heated via the Joule effect, (ii) the flow pattern identifies the resident axis of the defect with respect to the current injection, (iii) it is not affected by the surface morphology as the bulk laminate is heated via its cross sectional area and not via its interrogated surface and (iv) requires considerably less energy for the damage inspection; the total energy input for the LVI damage identification with current injection is 5 Joule compared to 20 kJ for the optical excitation.

For both 3J and 4J impact damage energies, the delaminations identified by the C-scanning method and the CT cross sectional representations appear as dark areas with both thermographic methods. As expected, the 3J impact energy resulted to smaller damaged area than in the case of 4J impact (Figs.9d, 10d, 11d and 12d). Similar behaviour was noticed for both the plain and CNT modified

matrix matters. In the case of the 4J impact damage, especially for the CNT modified specimen, the thermographic imprint of damage is manifested as two dark spots in the vicinity of the impacted area. As should be noted, the attainment of a uniform excitation field in the space domain through the optimisation of the current modulation protocol is indispensable. It is also noteworthy that the directionality of the current path as dictated by the symmetry of the material was clearly observed in all the IrT current injection phase images (Fig.9-12d). More analytically, at the current injection sides, constant phase thermographs exhibit increased thermal wave emission. This is directly attributed to the contact resistance of the electrodes [29]. Following, the phase images reveal reduced thermal wave activity on an envelope which surrounds the impact damage, revealing the thermal flow disturbance around the induced electrical discontinuity. It is believed that this effect is due to the combination of the plane electrical anisotropy of the material, i.e. the direction of the reinforcing fibres which define the paths of maximum conductivity and the current injection axis . It is also worth noting again, that the electrical induced thermal stimulation is not sensitive to the weaving pattern, as has been observed in other cases of thermal simulation [10].

6. Conclusions

The main objective of the paper was to develop a novel current injection thermographic technique for the detection of damage in composite laminates. The efficiency of the proposed methodology was tested in LVI damaged cross ply composite plates, and cross validated with optical thermography, C-scan and Computer Tomography (CT). Both live and pulse phase thermography was employed. Within the purpose of the study was to define the minimum current injection energy which would yield an acceptable resolving ability with current injection PPT.

The composite plates subjected to LVI of 3J and 4J.The performed impact energy levels did not lead to penetration of the laminates. In both impact energy level cases, the induced damage was identified. The major challenges for the application of the method were (i) the minimisation of the contact resistance at the current injection sites (ii) the uniform thermal stimulation of the composite structures so as to clearly pinpoint the internal characteristics which were imposed by LVI and (iii) the optimisation of the current injection protocol so as to avoid overheating and efficiently record the transient thermal gradient on the surface of the laminate.

Thermal stimulation was significantly affected by the electrical anisotropy of the composite laminates. The incorporation of the CNT conductive nanophase led in the clear thermal imprint of the current flow disturbance induced by the impact damage. This effect was manifested by two cold elliptical spots on either side of the impact location along the current flow axis, which was less obvious in the case of the unmodified laminates. This effect was attributed to the enhanced though

thickness conductivity of the CNT enhanced laminate, and was particularly evident in the real time (or live) thermographic inspection of the transient temperature profile of the laminate surface during the current injection phase.

Appropriate current modulation was necessary in order to enhance the resolution of the phase images. The energy input required for the identification of LVI damage with more than 3 signal to noise ratio was three to four orders of magnitude less than the typical energy input required with optically excited PPT. The comparison of the current stimulated PPT images with typical optical PPT phase images as well as C-scans revealed that current injection is capable of pinpointing the damage. As in the case of live thermographic inspection, damage is manifested as a low excitation area within a ribbon of higher excitation, parallel to the path of the current injection.

Summarizing, a novel current injection thermographic technique developed in this work. The employed thermographic system proved its ability in identifying LVI damage in composite materials both in live and pulse phase modes.

Acknowledgements

The authors would like to thank Associate Prof. Stefanos Zaoutsos for providing the impact damage facilities located at the Dept. of Mechanical Engineering of the Technological Educational Institute of Larissa, Greece.

References

[1] Aggelis DG, Barkoula NM, Matikas TE, Paipetis AS. Acoustic structural health monitoring of composite materials : Damage identification and evaluation in cross ply laminates using acoustic emission and ultrasonics. Composites Science and Technology. 2011.

[2] Katerelos DTG, Paipetis A, Loutas T, Sotiriadis G, Kostopoulos V, Ogin SL. In situ damage monitoring of cross-ply laminates using acoustic emission. Plastics, Rubber and Composites. 2009;38:229-34.

[3] Talreja R. Fatigue of composite materials: Technomic Pub. Co.; 1987.

[4] Richardson MOW, Wisheart MJ. Review of low-velocity impact properties of composite materials. Composites Part A: Applied Science and Manufacturing. 1996;27:1123-31.

[5] Paipetis A, Katerelos DTG. Post-impact fatigue behavior of composite laminates : current and novel technologies for enhanced damage tolerance. New York: Novinka/Nova Science Publishers Inc.; 2010.

[6] Angelidis N, Irving PE. Detection of impact damage in CFRP laminates by means of electrical potential techniques. Composites Science and Technology. 2007;67:594-604.

[7] Meola C, Carlomagno GM. Impact damage in GFRP: New insights with infrared thermography. Composites Part A: Applied Science and Manufacturing. 2010;41:1839-47.

[8] Krstulovic-Opara L, Klarin B, Neves P, Domazet Z. Thermal imaging and Thermoelastic Stress Analysis of impact damage of composite materials. Engineering Failure Analysis. 2011;18:713-9.

[9] Maldague X. Applications of Infrared Thermography in NonDestructive Evaluation. In: Testing TiON, editor.: Pramod Rastogi
e-Journal of Nondestructive Testing & Ultrasonics; 2000. p. 591-609.

[10] Grammatikos SA, Kordatos EZ, Barkoula NM, Matikas TE, Paipetis AS. Innovative non-destructive evaluation and damage characterisation of composite aerostructures using thermography. Plastics, Rubber and Composites. 2011;40:342-8.

[11] Meola C, Carlomagno GM, Squillace A, Vitiello A. Non-destructive evaluation of aerospace materials with lock-in thermography. Engineering Failure Analysis. 2006;13:380-8.

[12] Meola C, Carlomagno GM. Recent advances in the use of infrared thermography. Measurement Science and Technology. 2004;15:R27-R58.
[13] Busse G. Nondestructive evaluation of polymer materials. NDT and E International. 1994;27:253-62.
[14] Reynolds WN. Nondestructive testing (NDT) of fibre-reinforced composite materials. Materials & Design. 1984;5:256-70.
[15] Reynolds WN. Recent European work on the NDT of composite materials. Materials & Design. 1988;9:183-91.
[16] Maldague X, Galmiche F, Ziadi A. Advances in pulsed phase thermography. Infrared Physics and Technology. 2002;43:175-81.
[17] Maldague X, Marinetti S. Pulse phase infrared thermography. Journal of Applied Physics. 1996;79:2694-8.
[18] Maldague X. Theory and practice of infrared technology for nondestructive testing: Wiley; 2001.
[19] Vavilov VP, Marinetti S. Pulsed phase thermography and fourier-analysis thermal tomography. Russian Journal of Nondestructive Testing. 1999;35:134-45.
[20] Sarasini F, Tirillò J, Valente M, Ferrante L, Cioffi S, Iannace S, et al. Hybrid composites based on aramid and basalt woven fabrics: Impact damage modes and residual flexural properties. Materials & Design. 2013;49:290-302.
[21] Tarim N, Findik F, Uzun H. Ballistic impact performance of composite structures. Composite Structures. 2002;56:13-20.
[22] Matemilola SA, Stronge WJ. Impact induced dynamic deformations and stresses in CFRP composite laminates. Composites Engineering. 1995;5:211-22.
[23] Katerelos DG, Paipetis A, Kostopoulos V. A simple model for the prediction of the fatigue delamination growth of impacted composite panels. Fatigue and Fracture of Engineering Materials and Structures. 2004;27:911-22.
[24] Sutherland LS, Guedes Soares C. Effects of laminate thickness and reinforcement type on the impact behaviour of E-glass/polyester laminates. Composites Science and Technology. 1999;59:2243-60.
[25] Gleiter A, Spiebberger C, Busse G. Lockin thermography with optical or Ultrasound excitation. Strojniski Vestnik/Journal of Mechanical Engineering. 2010;56:619-24.
[26] Liu J, Qin L, Tang Q, Wang Y. Experimental study of inspection on a metal plate with defect using ultrasound lock-in thermographic technique. Infrared Physics and Technology. 2012;55:284-91.
[27] Grammatikos SA, Kordatos EZ, Matikas TE, Paipetis AS. Real-Time Debonding Monitoring of Composite Repaired Materials via Electrical, Acoustic, and Thermographic Methods. J of Materi Eng and Perform. 2013:1-12.
[28] Shah AA, Ribakov Y. Non-destructive measurements of crack assessment and defect detection in concrete structures. Materials & Design. 2008;29:61-9.
[29] Kostopoulos V, Vavouliotis A, Karapappas P, Tsotra P, Paipetis A. Damage monitoring of carbon fiber reinforced laminates using resistance measurements. Improving sensitivity using carbon nanotube doped epoxy matrix system. Journal of Intelligent Material Systems and Structures. 2009;20:1025-34.
[30] Grammatikos SA, Paipetis AS. On the electrical properties of multi scale reinforced composites for damage accumulation monitoring. Composites Part B: Engineering. 2012;43:2687-96.
[31] Grammatikos SA, Paipetis AS. Electrical resistance and electrical potential studies for the detection and monitoring of damage in hybrid composites. 2012. p. 401-6.
[32] Vavouliotis A, Paipetis A, Kostopoulos V. On the fatigue life prediction of CFRP laminates using the Electrical Resistance Change method. Composites Science and Technology. 2011;71:630-42.
[33] Grammatikos SA, Gkikas G, Paipetis A. Monitoring strain and damage in multi phase composite materials using electrical resistance methods. 2011.
[34] Schulte K, Baron C. Load and failure analyses of CFRP laminates by means of electrical resistivity measurements. Composites Science and Technology. 1989;36:63-76.
[35] Grammatikos SA, Paipetis AS. On the electrical properties of multi scale reinforced composites for damage accumulation monitoring. Composites Part B: Engineering.
[36] Irving PE, Thiagarajan C. Fatigue damage characterization in carbon fibre composite materials using an electrical potential technique. Smart Materials and Structures. 1998;7:456-66.
[37] Todoroki A, Kobayashi H, Matuura K. Application of electric potential method to smart composite structures for detecting delamination. JSME International Journal, Series A: Mechanics and Material Engineering. 1995;38:524-30.
[38] Ueda M, Todoroki A. Asymmetrical dual charge EPCM for delamination monitoring of CFRP laminate. 2006. p. 1309-15.
[39] Wang S, Chung DDL. Apparent negative electrical resistance in carbon fiber composites. Composites Part B: Engineering. 1999;30:579-90.
[40] Abry JC, Bochard S, Chateauminois A, Salvia M, Giraud G. In situ detection of damage in CFRP laminates by electrical resistance measurements. Composites Science and Technology. 1999;59:925-35.
[41] Todoroki A. Electric resistance change method for cure/strain/damage monitoring of CFRP laminates. 2004. p. 1812-20.
[42] Gkikas G, Sioulas D, Lekatou A, Barkoula NM, Paipetis AS. Enhanced bonded aircraft repair using nano-modified adhesives. Materials & Design. 2012;41:394-402.

[43] Gkikas G, Paipetis A, Lekatou A, Barkoula NM, Sioulas D, Canflanca B, et al. Corrosion and environmental degradation of bonded composite repair. International Journal of Structural Integrity. 2013;4:67-77.
[44] Athanasopoulos N, Kostopoulos V. Resistive heating of multidirectional and unidirectional dry carbon fibre preforms. Composites Science and Technology. 2012;72:1273-82.
[45] Athanasopoulos N, Kostopoulos V. Prediction and experimental validation of the electrical conductivity of dry carbon fiber unidirectional layers. Composites Part B: Engineering. 2011;42:1578-87.
[46] Hung C-c, Dillehay ME, Stahl M. HEATER MADE FROM GRAPHITE COMPOSITE MATERIAL FOR POTENTIAL DEICING APPLICATION. Journal of Aircraft. 1987;24:725-30.
[47] Thostenson ET, Chou TW. Carbon Nanotube Networks: Sensing of Distributed Strain and Damage for Life Prediction and Self Healing. Advanced Materials. 2006;18:2837-41.
[48] Chen X, Dam MA, Ono K, Mal A, Shen H, Nutt SR, et al. A thermally re-mendable cross-linked polymeric material. Science. 2002;295:1698-702.
[49] Park JS, Kim HS, Thomas Hahn H. Healing behavior of a matrix crack on a carbon fiber/mendomer composite. Composites Science and Technology. 2009;69:1082-7.
[50] Park JS, Takahashi K, Guo Z, Wang Y, Bolanos E, Hamann-Schaffner C, et al. Towards development of a self-healing composite using a mendable polymer and resistive heating. Journal of Composite Materials. 2008;42:2869-81.
[51] Fosbury A, Wang S, Pin YF, Chung DDL. The interlaminar interface of a carbon fiber polymer-matrix composite as a resistance heating element. Composites Part A: Applied Science and Manufacturing. 2003;34:933-40.
[52] Böger L, Wichmann MHG, Meyer LO, Schulte K. Load and health monitoring in glass fibre reinforced composites with an electrically conductive nanocomposite epoxy matrix. Composites Science and Technology. 2008;68:1886-94.
[53] Gao L, Thostenson ET, Zhang Z, Byun JH, Chou TW. Damage monitoring in fiber-reinforced composites under fatigue loading using carbon nanotube networks. Philosophical Magazine. 2010;90:4085-99.
[54] Gao L, Thostenson ET, Zhang Z, Chou TW. Sensing of damage mechanisms in fiber-reinforced composites under cyclic loading using carbon nanotubes. Advanced Functional Materials. 2009;19:123-30.
[55] Park J-M, Kim D-S, Kim S-J, Kim P-G, Yoon D-J, DeVries KL. Inherent sensing and interfacial evaluation of carbon nanofiber and nanotube/epoxy composites using electrical resistance measurement and micromechanical technique. Composites Part B: Engineering. 2007;38:847-61.
[56] Gkikas G, Barkoula NM, Paipetis AS. Effect of dispersion conditions on the thermo-mechanical and toughness properties of multi walled carbon nanotubes-reinforced epoxy. Composites Part B: Engineering. 2012.
[57] Bourlinos AB, Georgakilas V, Zboril R, Sterioti TA, Stubos AK. Liquid-Phase Exfoliation of Graphite Towards Solubilized Graphenes. Small. 2009;5:1841-5.
[58] Kulkarni R, Ochoa O. Transverse and longitudinal CTE measurements of carbon fibers and their impact on interfacial residual stresses in composites. Journal of Composite Materials. 2006;40:733-54.
[59] Rogers K, Kingston-Lee D, Phillips L, Yates B, Chandra M, Parker S. The thermal expansion of carbon-fibre reinforced plastics. Journal of Materials Science. 1981;16:2803-18.
[60] Takahashi K, Hahn HT. Investigation of temperature dependency of electrical resistance changes for structural management of graphite/polymer composite. Journal of Composite Materials. 2011;45:2603-11.
[61] Suk JW, Kitt A, Magnuson CW, Hao Y, Ahmed S, An J, et al. Transfer of CVD-grown monolayer graphene onto arbitrary substrates. ACS Nano. 2011;5:6916-24.
[62] Poeller M, Chung DDL. Effect of heating on the structure of an adhesive joint, as indicated by electrical resistance measurement. Journal of Adhesion. 2003;79:549-57.
[63] Wang S, Kowalik DP, Chung DDL. Effects of the temperature, humidity, and stress on the interlaminar interface of carbon fiber polymer-matrix composites, studied by contact electrical resistivity measurement. Journal of Adhesion. 2002;78:189-200.
[64] Gengler RYN, Veligura A, Enotiadis A, Diamanti EK, Gournis D, Józsa C, et al. Large-yield preparation of high-electronic-quality graphene by a langmuir-schaefer approach. Small. 2010;6:35-9.
[65] Bourlinos AB, Gournis D, Petridis D, Szabó T, Szeri A, Dékány I. Graphite oxide: Chemical reduction to graphite and surface modification with primary aliphatic amines and amino acids. Langmuir. 2003;19:6050-5.
[66] Stergiou DV, Stergiopoulos T, Falaras P, Prodromidis MI. Solid redox polymer electrolyte-based amperometric sensors for the direct monitoring of ozone in gas phase. Electrochemistry Communications. 2009;11:2113-6.
[67] Grammatikos S, Kordatos E, Barkoula NM, Matikas T, Paipetis A. Repair integrity monitoring of composite aerostructures using thermographic imaging. 2010.

List of figures

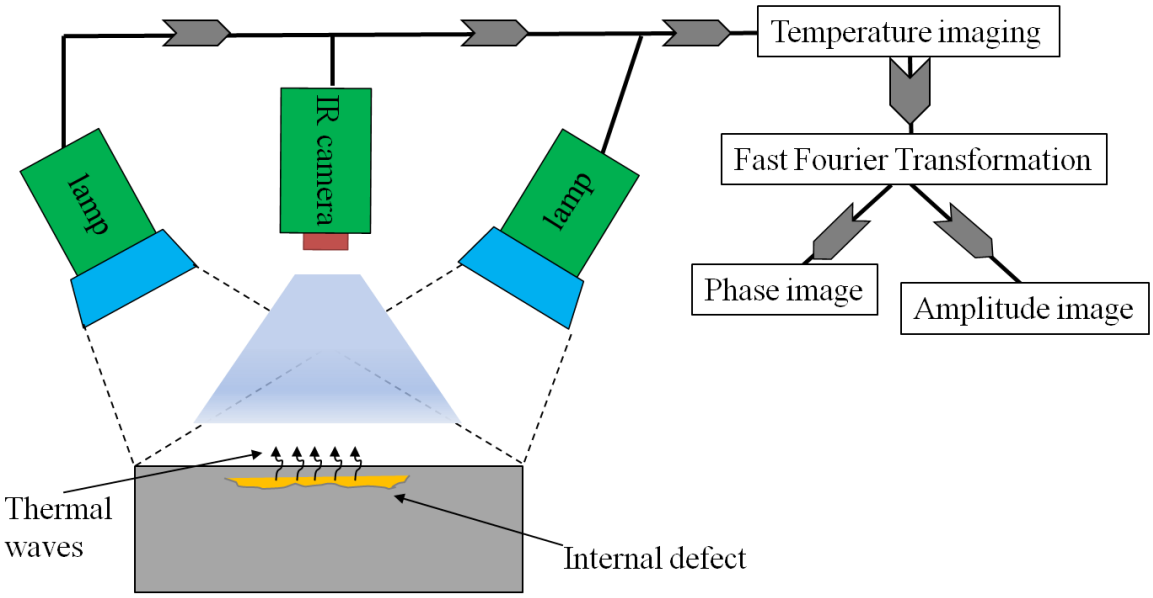

Figure 1. Pulsed phase thermography; optical excitation mode.

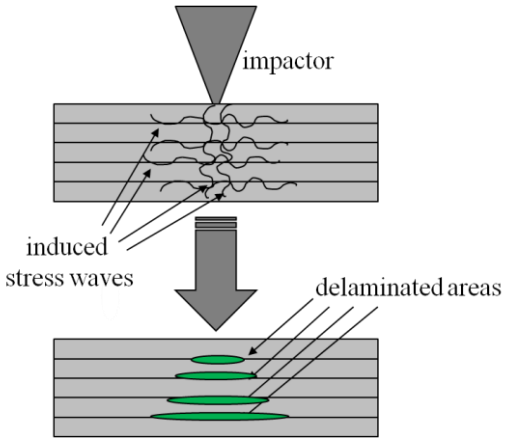

Figure 2. Low velocity impact damage concept; invisible defects.

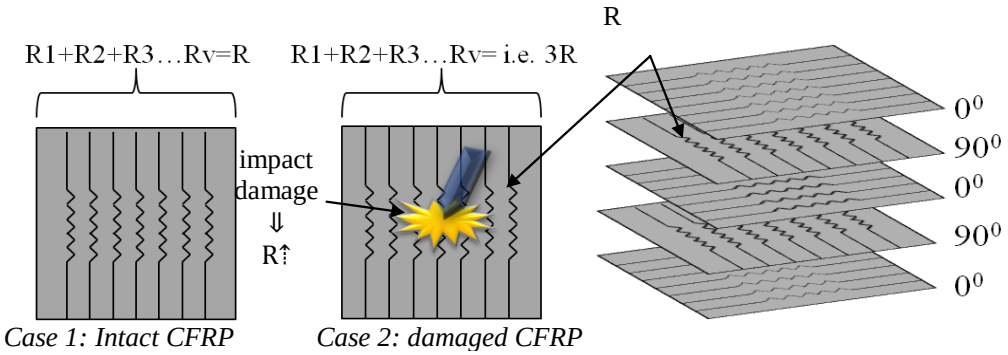

Figure 3.
Mechanical models of Carbon fibre fabrics; array of electrical resistances: (a) carbon fibre layers; intact case (1) and damaged case (2), (b) lay-up of a cross-ply CFRP laminate.

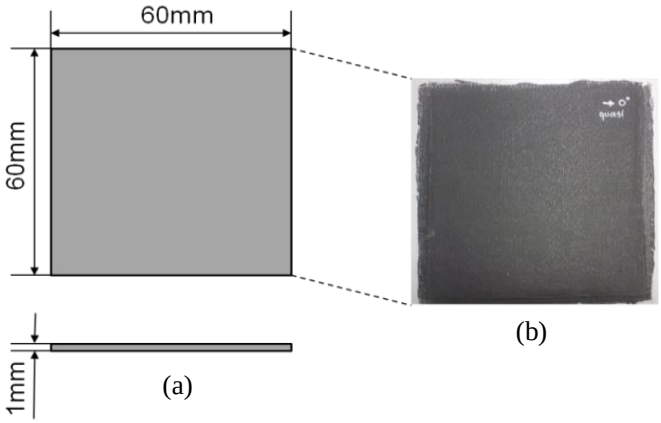

Silver adhesive paint at the edges and cross section

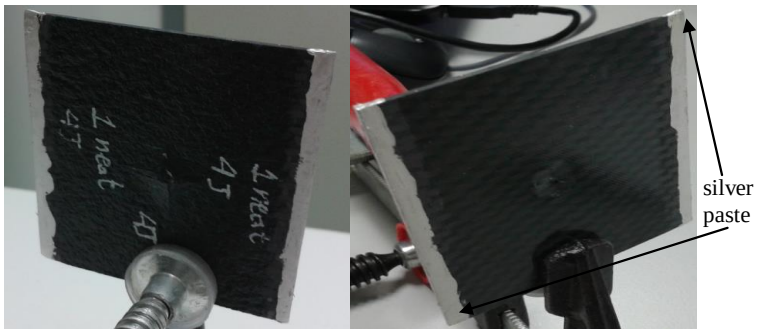

Silver loaded adhesive tape at the edges and cross section

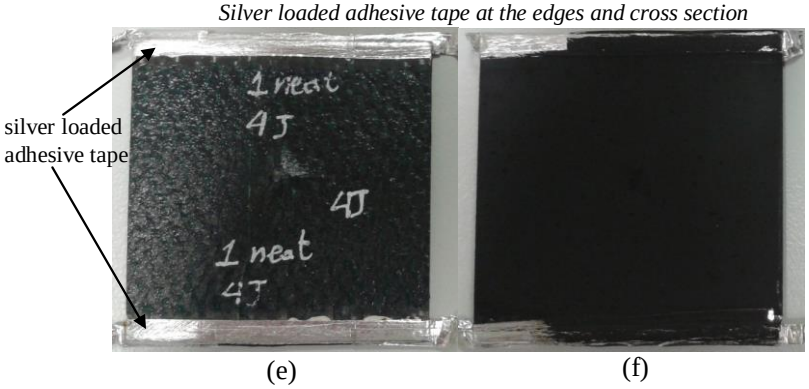

Figure 4. (a) CFRP specimen configuration, (b) CFRP laminate (c-d) snapshot during specimen preparation.

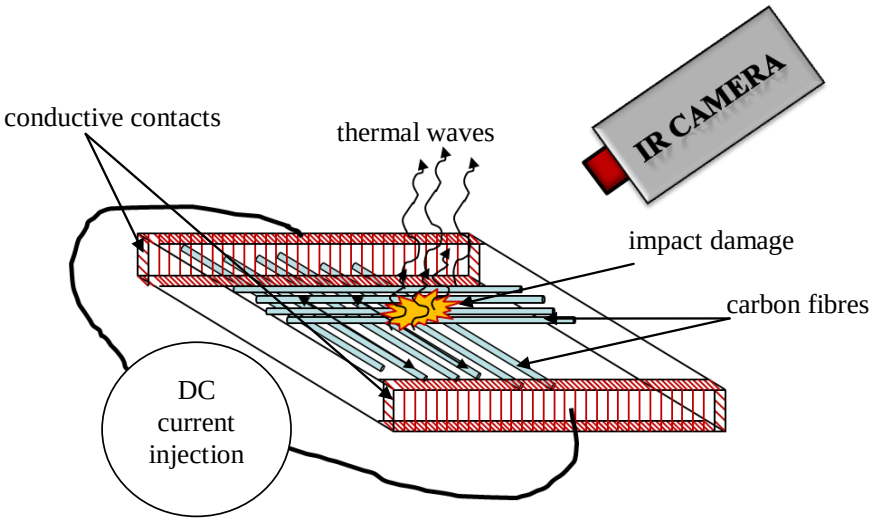

Figure 5. Current injection experimental setup configuration

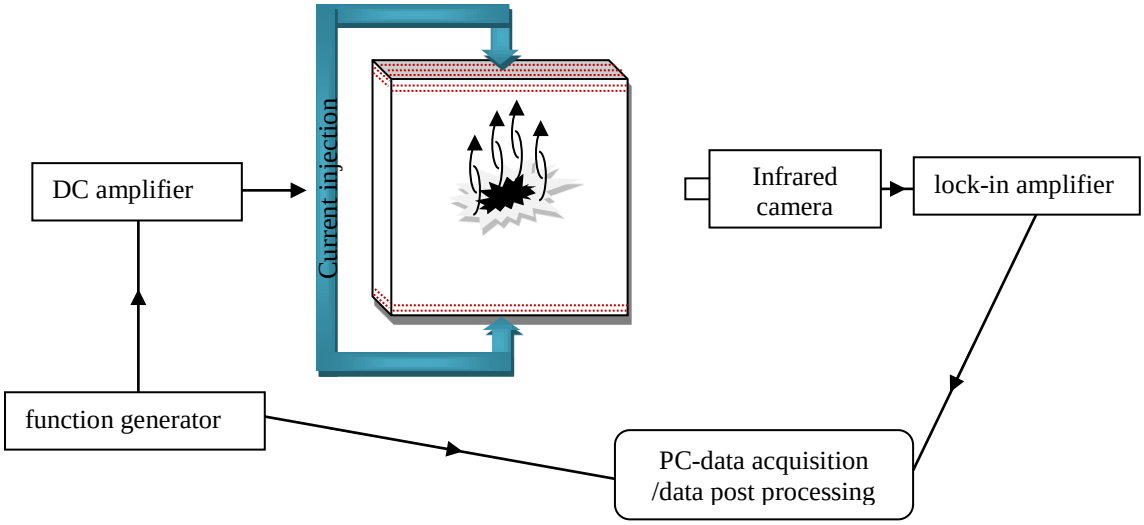

Figure 6. Outline of the experimental setup.

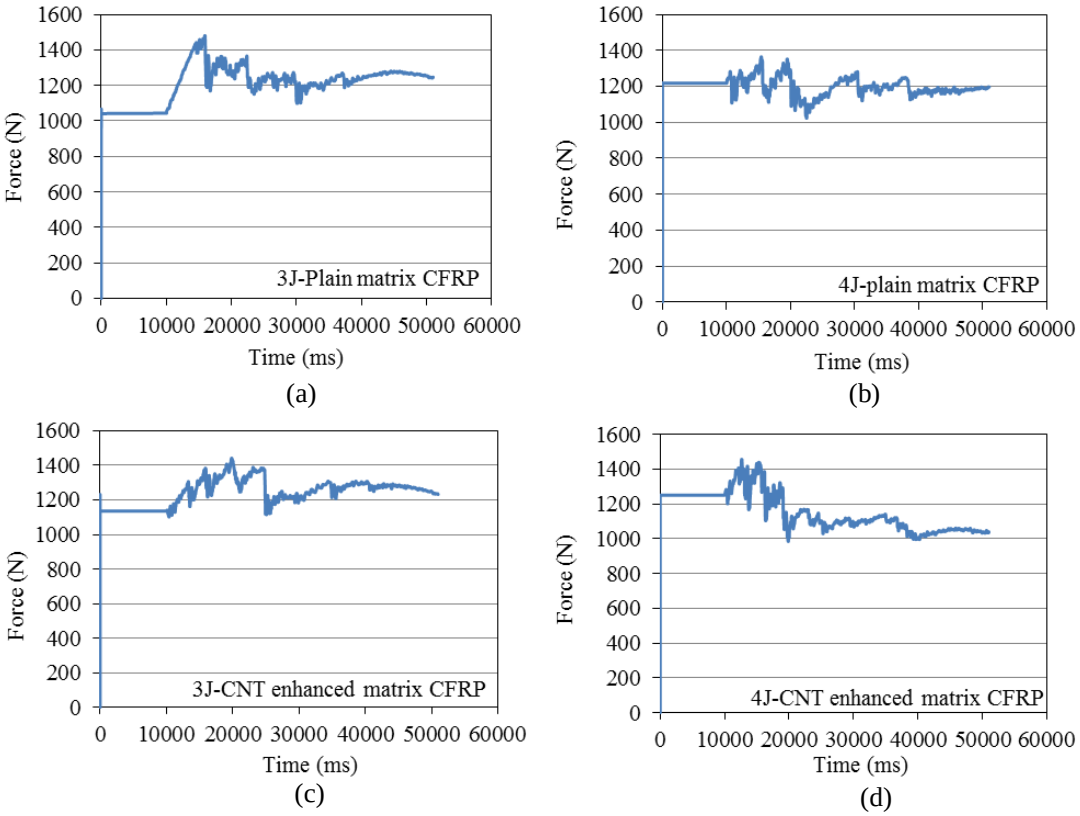

Figure 7. Force vs. time graphs for both plain (a,b) and CNT modified matrix specimens (c,d).

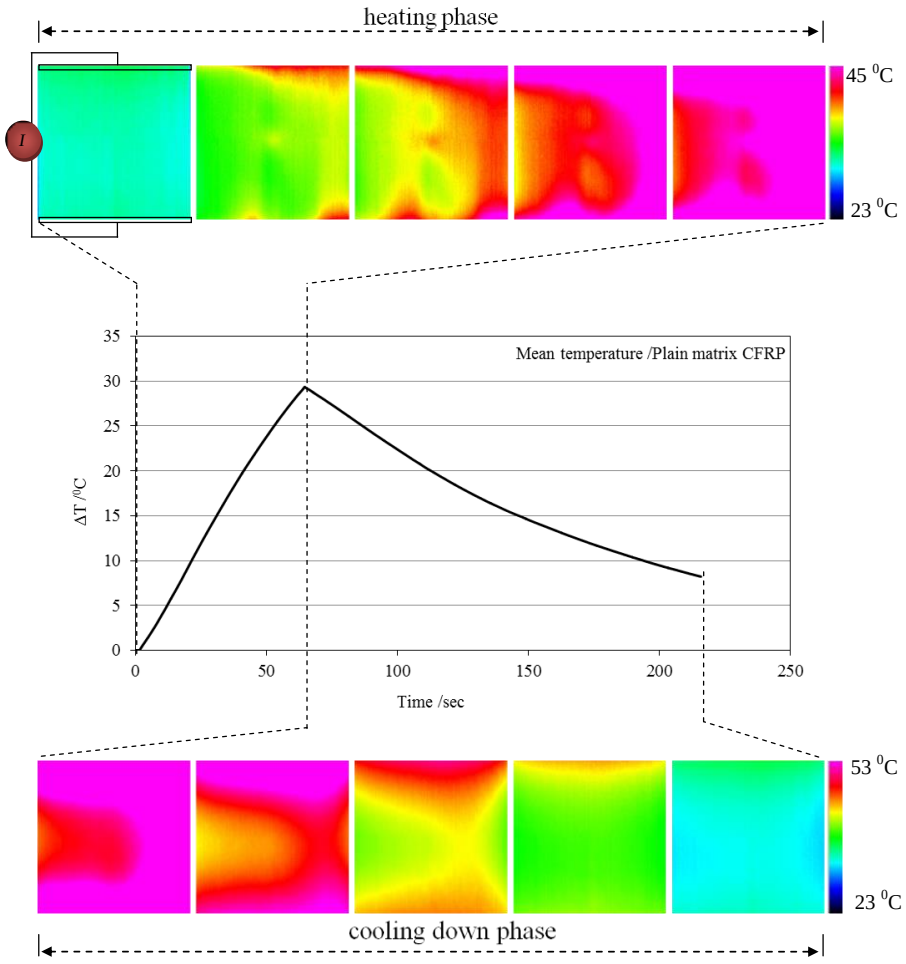
heating phase
I
45 ^{0}C
23 ^{0}C
Mean temperature /Plain matrix CFRP
ΔT /^{0}C
35
30
25
20
15
10
5
0
0
50
100
150
200
250
Time /sec
53 ^{0}C
23 ^{0}C
cooling down phase

(a)

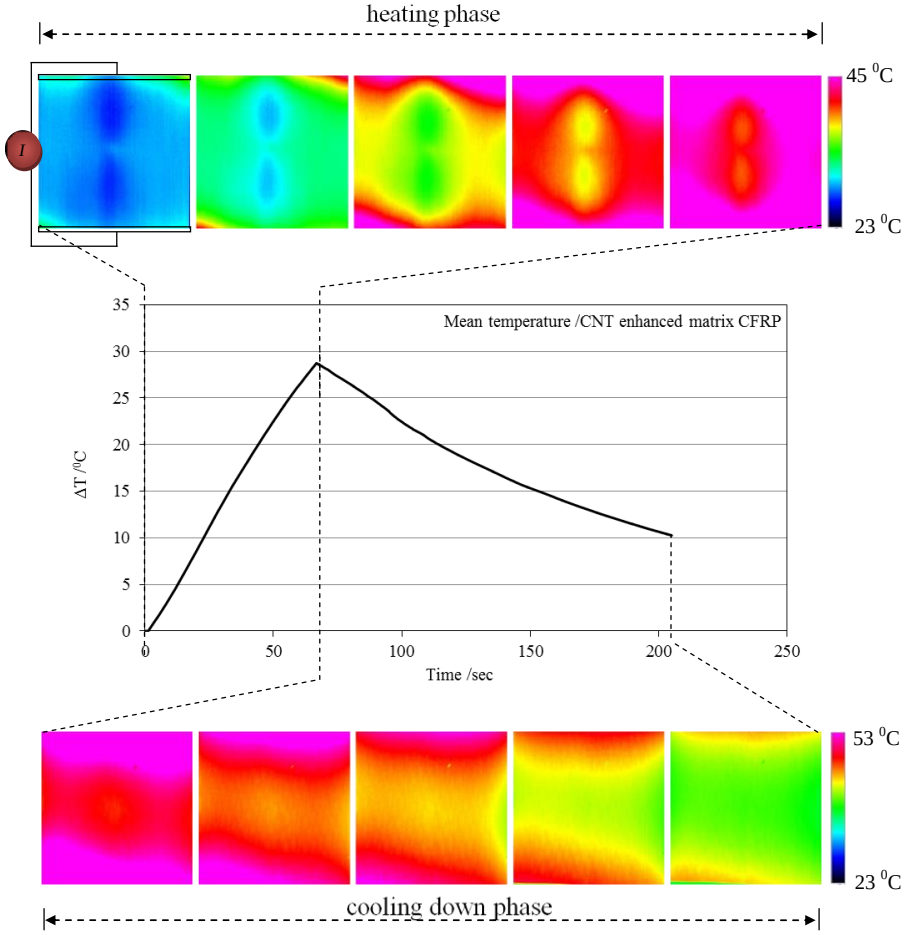

(b)

Figure 8. Thermal stimulation procedure; temperature profile and representative thermographs (live mode) of the reference (a) and CNT modified (b) CFRP laminates when fixed - amplitude DC current is injected in the composites.

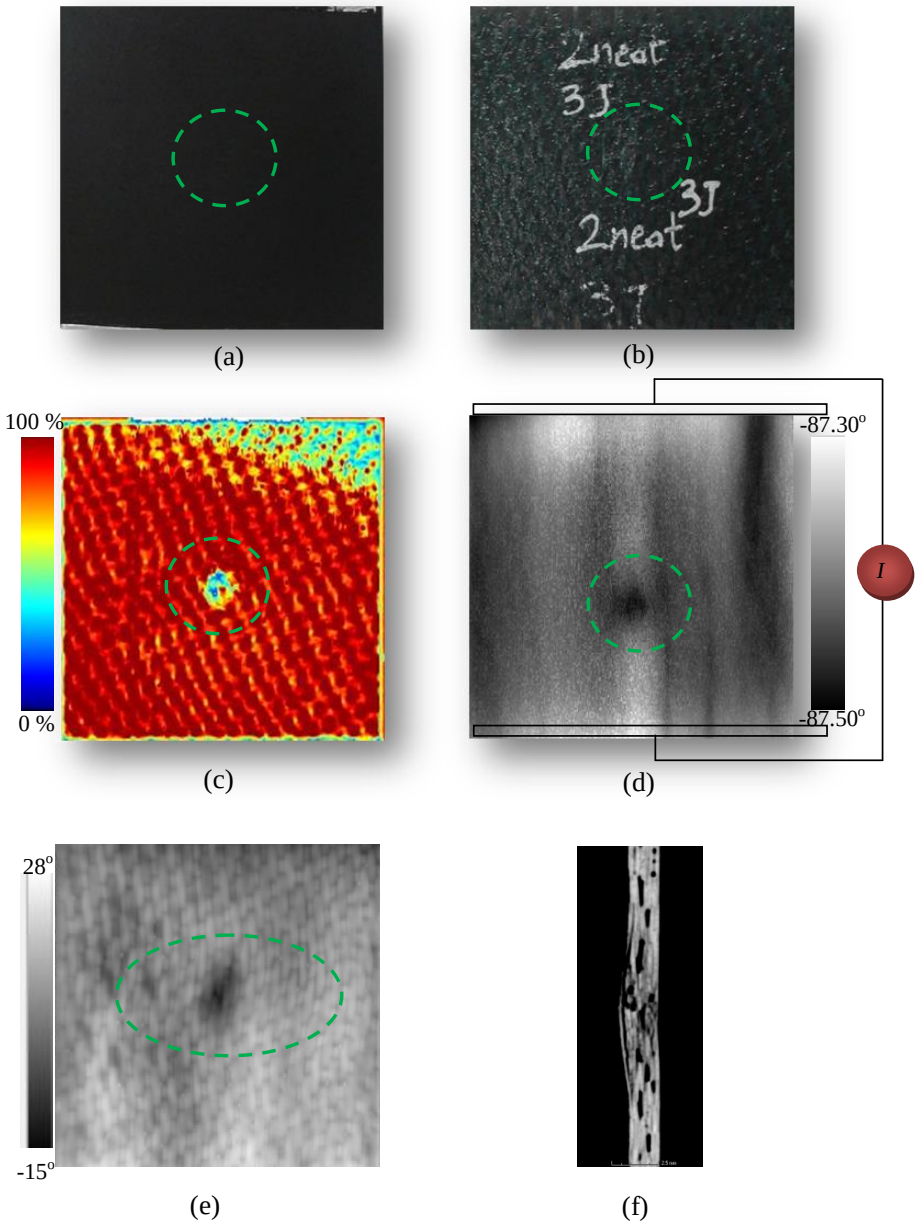

Figure 9. Plain epoxy matrix CFRP - 3J impact damage; (a) top (front) side of the coupon, (b) bottom (back) side of the coupon, (c) C-scan imaging, (d) IrT phase image (current injection excitation) (e) IrT phase image (IR optical excitation) (f) CT middle Cross section

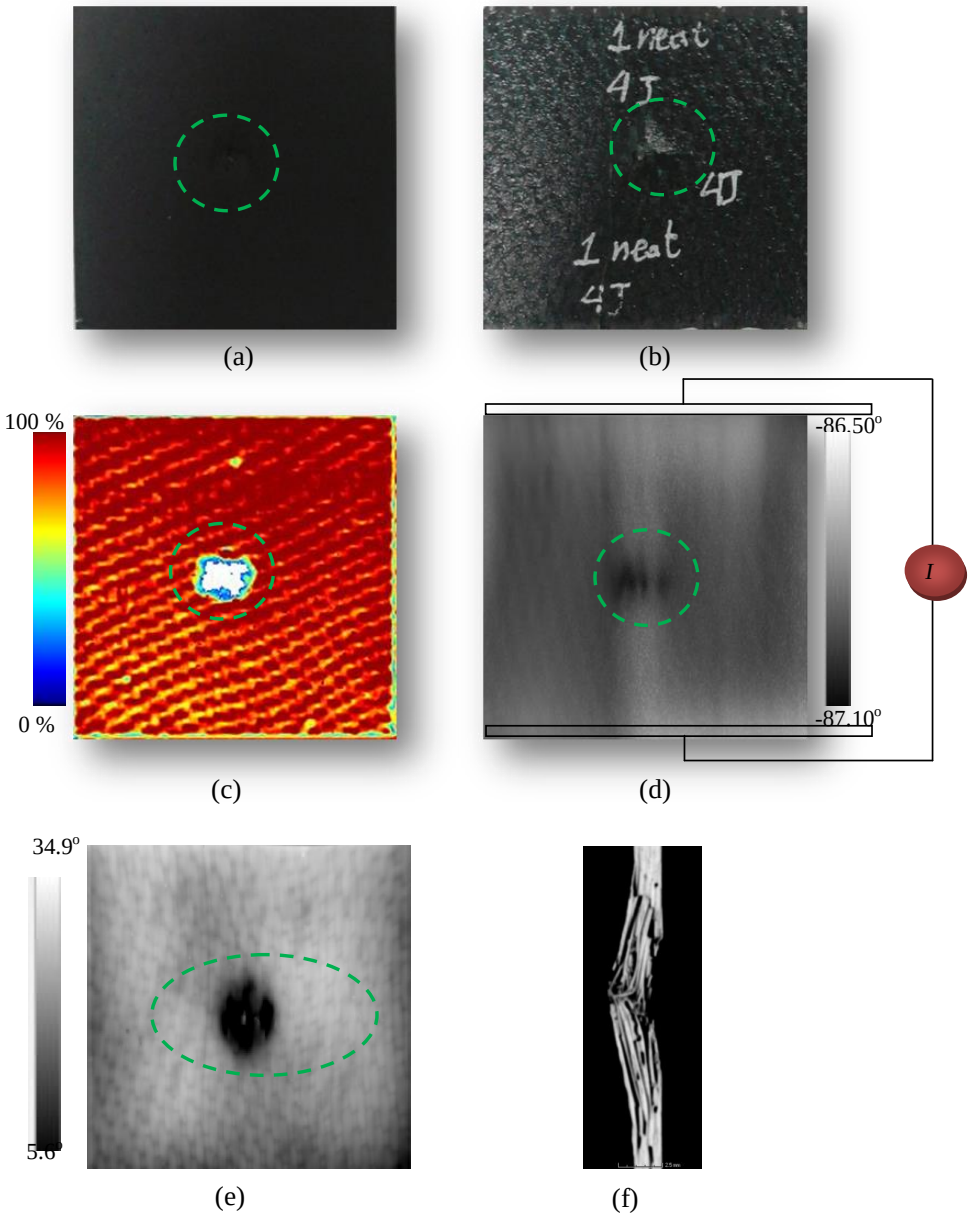

Figure 10. Plain epoxy matrix CFRP - 4J impact damage; (a) top (front) side of the coupon, (b) bottom (back) side of the coupon, (c) C-scan imaging, (d) IrT phase image (current injection excitation) (e) IrT phase image (IR optical excitation) (f) CT middle Cross section

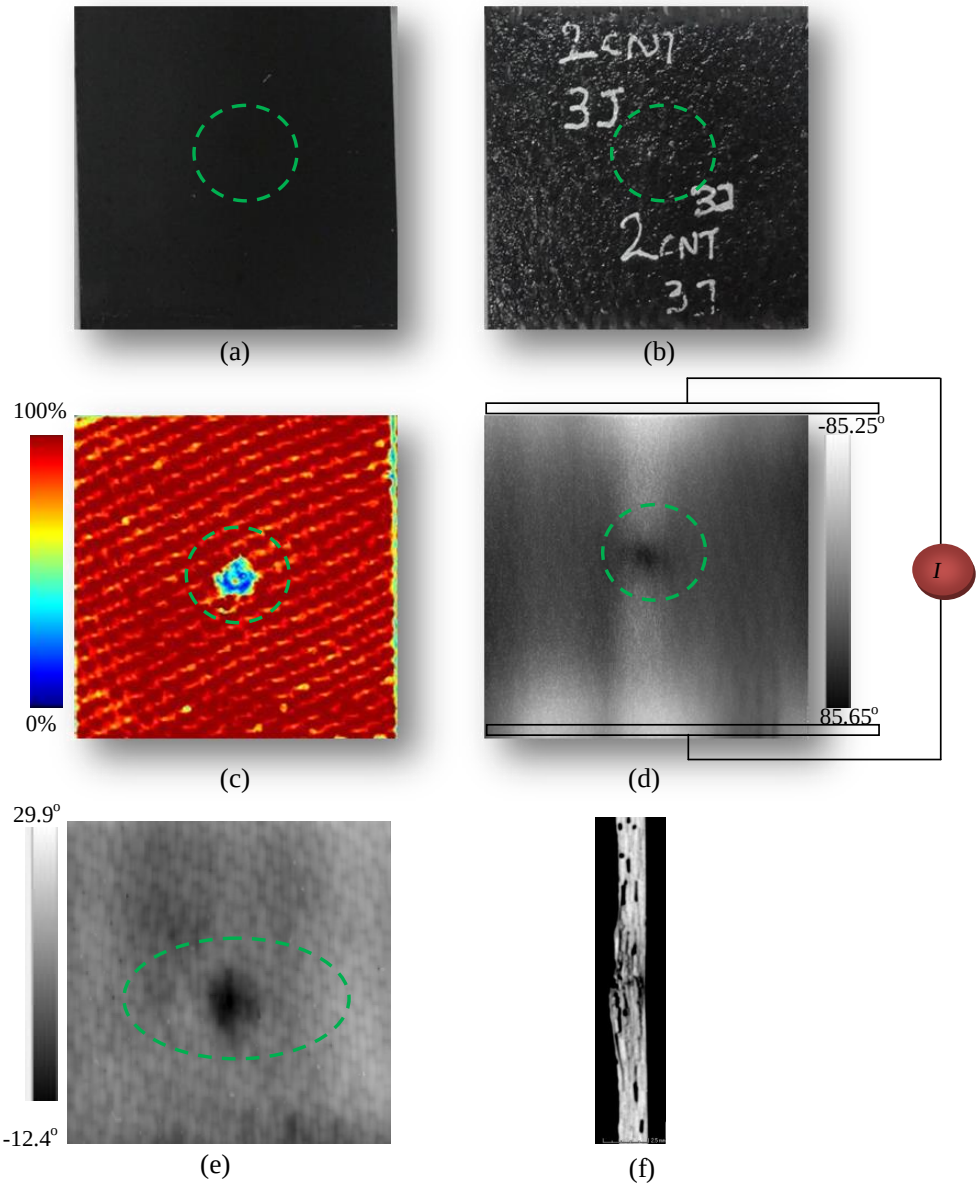

Figure 11. CNT modified epoxy matrix CFRP - 3J impact damage; (a) top (front) side of the coupon, (b) bottom (back) side of the coupon, (c) C-scan imaging, (d) IrT phase image (current injection excitation) (e) IrT phase image (IR optical excitation) (f) CT middle Cross section

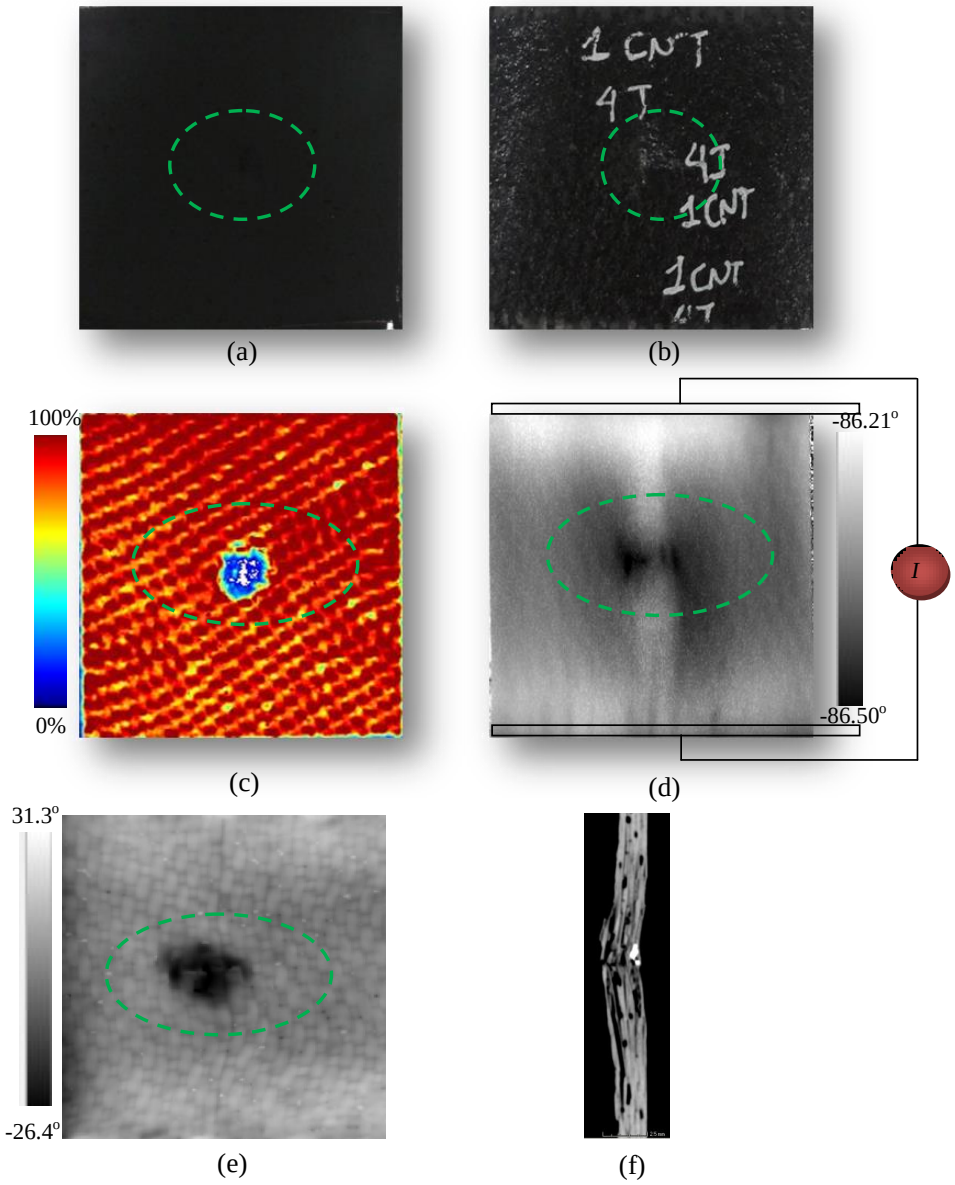

Figure 12. CNT modified epoxy matrix CFRP - 4J impact damage; (a) Top (front) side of the coupon, (b) bottom (back) side of the coupon, (c) C-scan imaging, (d) IrT phase image (current injection excitation) (e) IrT phase image (IR optical excitation) (f) CT middle Cross section